2019

Direct observation of structure-assisted filament splitting during ultrafast multiplepulse laser ablation

Feifei Wang

Changji Pan

Jingya Sun

Qingsong Wang

Yongfeng Lu

See next page for additional authors

Authors
Feifei Wang, Changji Pan, Jingya Sun, Qingsong Wang, Yongfeng Lu, and Lan Jiang

Research Article | Vol. 27, No. 7 | 1 Apr 2019 | OPTICS EXPRESS 10050
Optics EXPRESS

Direct observation of structure-assisted filament splitting during ultrafast multiple-pulse laser ablation

FEIFEI WANG,[1,3] CHANGJI PAN,[1,3] JINGYA SUN,[1] QINGSONG WANG,[1] YONGFENG LU,[2] AND LAN JIANG[1,*]

[1]*Laser Micro/Nano-Fabrication Laboratory, School of Mechanical Engineering, Beijing Institute of Technology, Beijing 100081, China*
[2]*Department of Electrical Engineering, University of Nebraska-Lincoln, Lincoln, Nebraska 68588-0511, USA*
[3]*These authors contributed equally to this work*
[*]*jianglan@bit.edu.cn*

Abstract: Laser-induced plasma evolution in fused silica through multipulse laser ablation was studied using pump-probe technology. Filament splitting was observed in the early stage of plasma evolution (before ~300 fs). This phenomenon can be attributed to competition between laser divergent propagation induced by a pre-pulse-induced crater and the nonlinear self-focusing effect. This effect was validated through simulation results. With the increasing pulse number, the appearance of filament peak electron density was postponed. Furthermore, a second peak in the filament and peak position separation were observed because of an optical path difference between the lasers propagating from the crater center and edge. The experimental results revealed the influence of a prepulse-induced structure on the energy distribution of subsequent pulses, which are essential for understanding the mechanism of laser–material interactions, particularly in ultrafast multiple-pulse laser ablation.

1. Introduction

Femtosecond laser ablation has become crucial because it has a large amount of practical applications in numerous scientific [1–4], medical [5,6], and industrial fields [7]. However, the potential is still limited because of the complexity of the ablation process, which involves various mechanisms such as energy deposition [8,9], energy transfer [10], and energy relaxation [11]. During the ablation process, energy deposition from the laser to material is crucial because it determines ablation results. Kerse et al. particularly aimed to control the energy deposition process and realized thermal-damage-free ablation by adjusting laser repetition rates [12]. Wang et al. used cylindrical focusing and rapid scans to form a large area of ripples through spontaneous energy deposition [13]. For multipulse ablation, energy deposition may be affected by numerous factors, such as shielding [14], saturation [15], and collateral damage [16]. A structure ablated by a pulse can strongly reshape the subsequent pulses, thus spatially redistributing energy deposition and affecting the subsequent processes (e.g., plasma generation [15] and shockwave evolution [17,18]). Photon–electron interaction is the first step of energy deposition during laser ablation [19] and is thus the most crucial step during multipulse ablation [20]. Some previous works have been carried out to investigate the mechanism of multipulse ablation in terms of numerical model and final damage structures [21,22]. However, few studies have focused on this dynamic behavior under multipulse irradiation; moreover, the related mechanisms have not been completely elucidated. Therefore, to reveal the mechanism of interaction between the laser and materials and to further improve ablation results during multiple-pulse laser ablation, electron dynamics driven by laser energy deposition must be studied in real time.

#358835 https://doi.org/10.1364/OE.27.010050
Journal © 2019 Received 14 Feb 2019; revised 14 Mar 2019; accepted 14 Mar 2019; published 26 Mar 2019

Optics EXPRESS

In this study, laser-induced plasma evolution in fused silica through multipulse ablation and the effect of a prepulse-induced crater on the subsequent laser field were studied using pump-probe technology. The splitting of a filament was observed in the early stage of plasma evolution (before ~300 fs) because the prepulse-induced crater reshaped the subsequent laser field; filament splitting was attributed to competition between divergent propagation of the laser caused by refraction and the self-focusing effect. Finite-different time-domain (FDTD) simulation of the laser field was performed to verify this phenomenon. The lasers propagating from the edge and center of the crater were focused over time because of the self-focusing effect. During the subsequent propagating process with multiple pulses, two peaks of filament electron density were observed at different delay times because of an optical path difference between the pulses from the two aforementioned paths. Finally, divergent propagation of the laser generated a hole with branches. When the pulse number was higher than a particular value (e.g., 200 in the proposed experiment), the laser-induced electron density saturation was observed, illustrating that the hole branch structures were unchanged.

2. Experimental setup

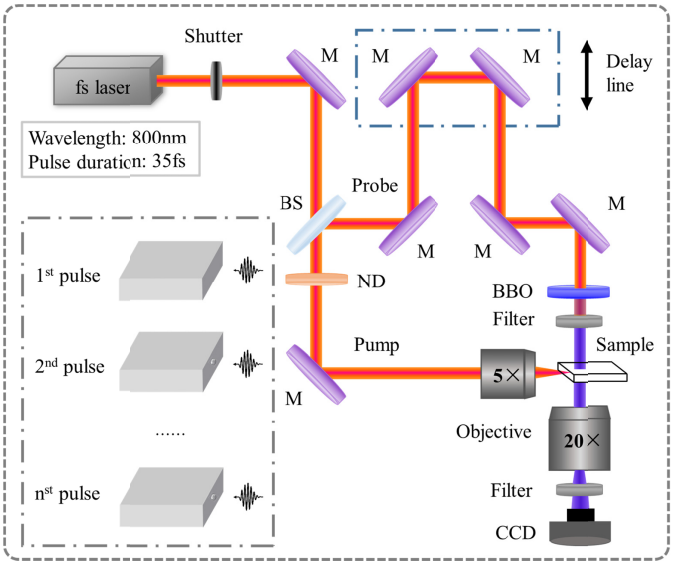

Fig. 1. Schematic of the pump-probe imaging setup. M: mirror; BS: beam splitter; and ND: neutral density filter.

Figure 1 presents a schematic of the pump-probe imaging setup based on our previous studies [17,23]. The output of a Ti:sapphire femtosecond laser regenerative amplifier (Spectra-Physics Spitfire Ace) at 800 nm with a pulse duration of 35 fs was divided into two beams by using a beam splitter. One of the two beams was frequency doubled by a beta barium borate crystal to generate a probe beam, whereas the other beam was focused using a 5 × , 0.15 numerical aperture (NA) objective (Olympus, Inc.) on the side surface of the fused silica to generate a pump beam. To probe plasma evolution in the sample, the probe beam and pump beam were placed perpendicular to each other for forming a side view. Pump energy was controlled by a neutral density filter and the spot size is 12 μm. The probe beam was delayed using an optical delay line to probe the sample at different delay times. Finally, a time-resolved transmissivity image of plasma was imaged on a charge-coupled device (CCD) with a 20 × , 0.45 NA objective (Olympus, Inc.). The sample was a piece of fused silica with a size of 10 mm × 10 mm × 1 mm, which is polished on four surfaces (two front surfaces and two side surfaces). To suppress disturbance caused by the pump beam (800 nm) and plasma radiation, a 400-nm bandpass filter was used in front of the CCD. A sequence of images was

Optics EXPRESS

recorded after each pulse ablation to study the dynamics of multipulse ablation. Moreover, an image without laser irradiation was recorded as a reference signal to obtain transmissivity shadowgraphs for each pulse ablation. In addition, ablation crater morphology was determined using an atomic force microscope (AFM, Bruker, Inc.).

3. Results and discussion

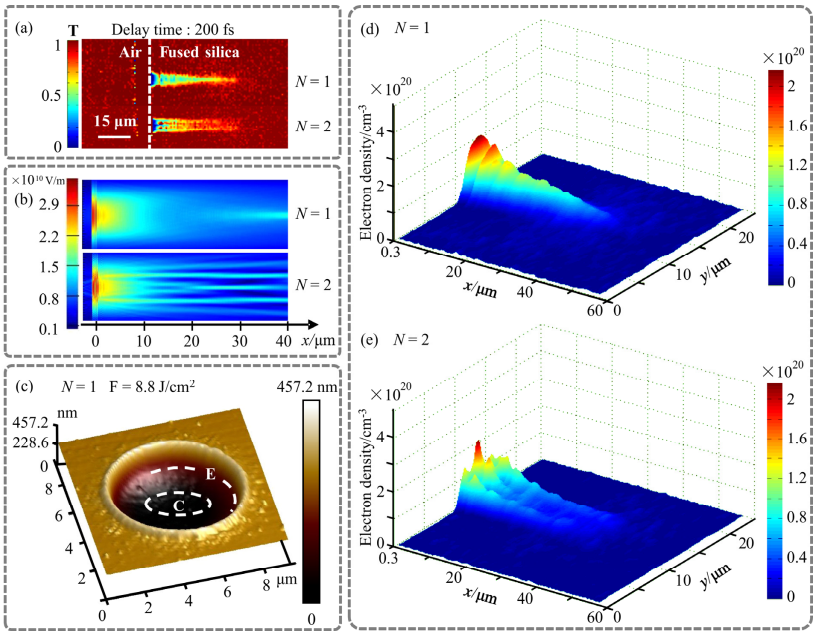

Fig. 2. (a) Time-resolved transmission of femtosecond laser-induced plasma evolution caused by the first pulse ($N = 1$) and second pulse ($N = 2$) in fused silica with a fluence of 8.8 J/cm^2 at 200 fs; (b) FDTD simulation of the laser field considering the Kerr effect in fused silica with the first and second pulses; the laser propagates in the direction of the x-axis, and the sample surface is $x = 0$; (c) AFM morphology of the crater caused by the first pulse, where "E" and "C" are the edge and the center area of the crater; and (d) and (e) spatial distribution map of electron density extracted from (a).

When a pump pulse was propagating inside the sample, the laser-induced free electron plasma would absorb the probe beam [24]. Figure 2(a) presents a time-resolved transmission of femtosecond laser-induced plasma under the first and second pulse irradiations in fused silica, where a colorbar represents transmissivity from 0 to 1. The fluence of each pulse was 8.8 J/cm^2, and the delay time of 200 fs was selected to compare the difference between filaments of the first and second pulses. The slight asymmetry of the filament was attributed to the beam quality. When the first pulse propagated into the sample, the laser was gradually focused, and a plasma filament was formed through the laser–material interaction. In the case of second pulse irradiation ($N = 2$), a distinct plasma filament splitting phenomenon was observed, which was evidently different from the first pulse-induced plasma ($N = 1$). The splitting phenomenon is similar to final crater shape in previous works [21,22] and needs to be further explained. The formation of the plasma filament for the first pulse ($N = 1$) was attributed to the self-focusing effect caused by the optical Kerr effect. The optical Kerr effect is a nonlinear change in the refractive index in the presence of strong electromagnetic fields. During the irradiation of a sample by an intense laser, the refractive index of sample n is not constant. Thus, the refractive index is not only related to the laser frequency (i.e., laser dispersion) but also dependent on laser intensity as $n = n_0 + n_2 I(r, t)$. Here, n_0 and n_2 are the original linear refractive index of fused silica and the nonlinear Kerr coefficient associated with the third-order susceptibility $\chi^{(3)}$, respectively, where $\chi^{(3)} = 4\varepsilon_0 c n_2 n_0^2/3$ (ε_0 is the

Optics EXPRESS

permittivity of vacuum and c is light speed in vacuum). Thus, an intense laser field with the Gaussian distribution of intensity generates an uneven Δn with the curvature of the wavefront similar to that of a lens. This effect is accumulative and can result in beam self-focusing [25]. The plasma filament is generated by balancing the self-focusing effect and defocusing of the beam in the presence of plasma [26].

In the case of second pulse irradiation, not only the aforementioned factors but also sample surface morphology affected laser propagation. The laser field of the second pulse was spatially reshaped by the crater generated using the first pulse ablation. Figure 2(c) shows the AFM morphology of the crater generated using the first pulse. When the second pulse reached the sample surface, the pulse was refracted by the crater. Because the refraction angle decreased when the light propagated from an optically thinner medium to an optically denser medium. In the initial stage of propagation, divergent propagation generated by refraction competed with the self-focusing effect. The slope was large on the edge of the crater ["E" area in Fig. 2(c)]; thus, the laser diverged from the original direction. The refractive index, Δn, changes slightly with the decreasing laser intensity. Divergent propagation effect of the laser was stronger than the self-focusing effect. However, the self-focusing effect was dominant in the central area ["C" area in Fig. 2(c)] because the crater had a relatively uniform bottom and the refractive index increased considerably with the increasing laser intensity. Therefore, these two parts of laser leaded to formation of filament splitting when they propagated into the sample. On the basis of acquired transmissivity, the electron density of laser-induced plasma can be calculated using the method proposed by Mao [27]. By using this method, an important parameter, e.g. plasma diameter, should be estimated. In the case of our experiment, the filament splitting phenomenon need to be considered. Thus, the electron density was calculated with different filament diameter in different areas. Besides, another important parameter, electron relaxation time, is also necessary to defined. For the sake of simplicity, we used the electron relaxation time as 0.2 fs, which is consistent with Mao [27] and our previous work [28]. Figures 2(d) and 2(e) present electron density spatial distribution extracted from Fig. 2(a) with pulse numbers N = 1 and 2, respectively. Electron density was calculated from a distance of 300 nm from the surface to ensure that electron density calculation was not affected by the pre-induced crater (with a depth of approximately 250 nm). Moreover, the split phenomenon could be observed from the spatial distribution.

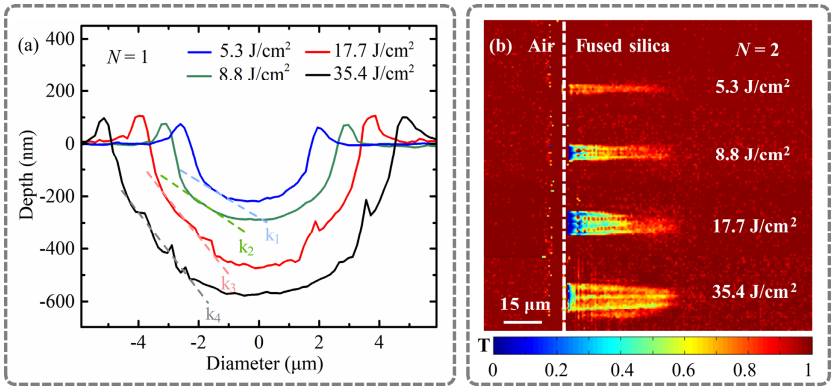

Fig. 3. (a) Cross-section morphology generated by the first pulse with fluences of 5.3, 8.8, 17.7, and 35.4 J/cm^2, and the slopes of the crater tangent line were k_1 = –68.3, k_2 = –76.2, k_3 = –143.2, and k_4 = –149.1; and (b) time-resolved transmission of femtosecond laser-induced plasma generated by the second pulse in fused silica with four fluences at 200 fs.

To validate the aforementioned explanation, FDTD simulation of the laser field was performed. Figure 2(b) presents laser fields of the first and second pulse irradiations. The surface morphology and Kerr effect were considered in this calculation. In the case of second pulse irradiation, the morphology of sample was extracted from AFM measurement [Fig.

Optics EXPRESS

2(c)]. The applied Kerr coefficient $n_2 = 3.54 \times 10^{-20}$ m^2/W was consistent with previous work [29]. The calculated distribution of the laser field was consistent with the distribution of laser-induced plasma obtained from the experiments.

In order to study the laser fluence effect on plasma filament splitting, experiments with different laser fluences were conducted. Figure 3(a) shows the cross-section morphology of craters generated by the first pulse with fluences of 5.3, 8.8, 17.7, and 35.4 J/cm^2. The increasing laser fluence gradually increased the diameter and depth of the crater. Furthermore, the slope of the crater tangent line increased. Accordingly, Fig. 3(b) compares the time-resolved transmission of femtosecond laser-induced plasma generated using the second pulse in fused silica with the four fluences. The plasma filament splitting phenomenon was increasingly evident with the increasing laser fluence, which validated the universality of this phenomenon.

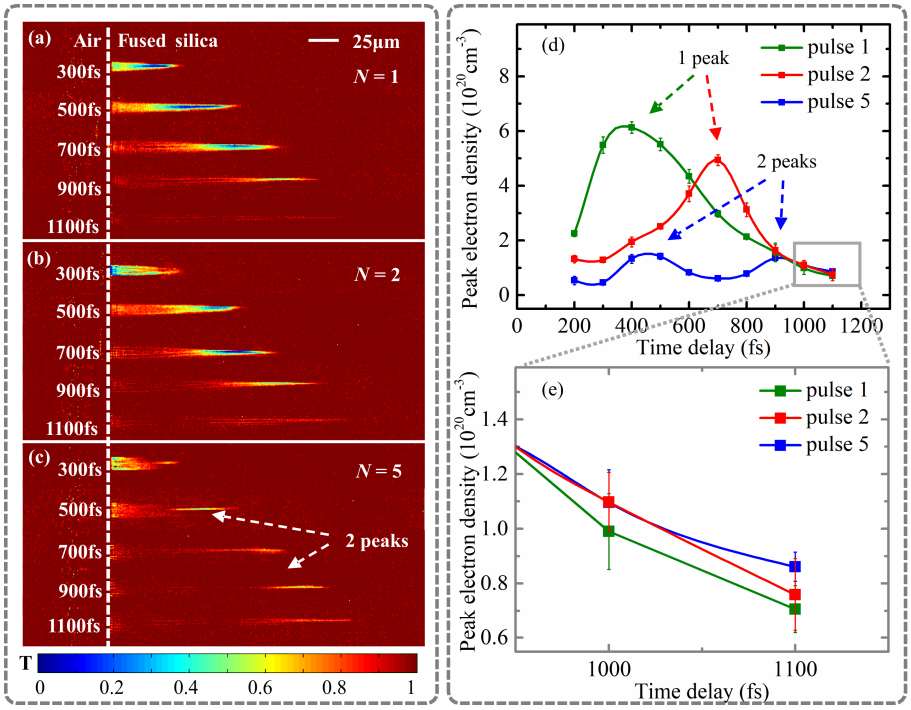

Fig. 4. Time-resolved transmission of femtosecond laser-induced plasma in fused silica with the (a) first pulse ($N = 1$), (b) second pulse ($N = 2$), (c) fifth pulse ($N = 5$), and (d and e) peak electron density evolution of center filament at delay times from 300 to 1100 fs with a fluence of 17.7 J/cm^2.

To investigate laser-induced plasma evolution with different pulses, time-resolved transmission of multipulse-induced plasma in fused silica were recorded. The transmitted shadowgraphs [Figs. 4(a)–4(c)] revealed the evolution of laser-induced plasma induced by the first, second, and fifth pulses. For the first pulse [Fig. 4(a)], typical plasma filament was formed by balancing self-focusing and plasma defocusing, and laser pulse intensity gradually weakened with time. The increasing pulse number [Fig. 4(b) and 4(c)] indicated that although the plasma filament was split in the initial stage of propagation, it refocused and recombined into one filament when the laser propagated the material because of the self-focusing effect. To further study this phenomenon, Figs. 4(d) and 4(e) were plotted to explain the evolution of peak electron density of center filament over time delay, which referred to the maximum value in spatial distribution at each time delay. Figure 4(d) shows that the corresponding time of the peak electron density was deferred backward with the increasing pulse number.

Optics EXPRESS

Furthermore, when the pulse number was higher than a particular value, two plasma density peaks were observed (blue line in Fig. 4(d)), which corresponded to bright filaments (i.e., low transmissivity) [Fig. 4(c)]. The appearance time difference of two peaks was related to the profile of the crater, which significantly changed the pulse path. The increasing pulse number increased the optical path difference between the pulses from the center and edge areas. The first and second peaks were attributed to the self-focusing of the pulse from the center and edge of the crater, respectively. To validate the phenomenon, the enlarged schematic of Fig. 4(d) is plotted in Fig. 4(e) to show the peak electron density extracted at time delays of 1000 and 1100 fs. Peak electron density was higher for $N = 5$ than for $N = 1$ and 2, which indicated that filament can maintain higher electron density for longer time. This difference was because the prepulse-induced crater increased the laser propagation distance of the pulse from the edge area, thus postponing the rate of electron decay.

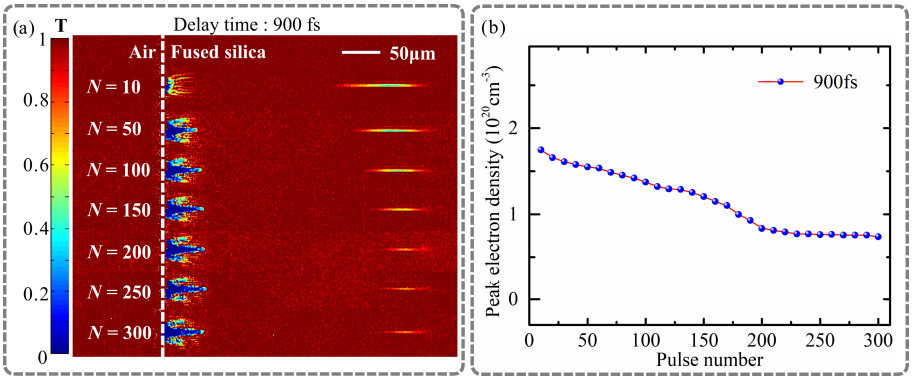

Fig. 5. (a) Time-resolved transmission of femtosecond laser-induced plasma in fused silica with 10–300 pulses and (b) peak electron density evolution at 900 fs with a fluence of 17.7 J/cm^2.

To further study the mechanism of multipulse ablation, the evolution of laser-induced plasma in fused silica was studied with the increasing number of pulses. Figure 5(a) shows time-resolved transmission of femtosecond laser-induced plasma with 10–300 pulses at 900 fs. A hole was gradually formed with two side branches in the cross-section view, which is indicated by a dark blue area in Fig. 5(a). With the increasing number of pulses, the depth of the hole increased, and side branches were gradually formed. Peak electron density of center filament at 900 fs from N = 10–300 was measured and plotted in Fig. 5(b). When the pulse number was higher than 200, peak electron density was unchanged. This behavior illustrated the invariability of side branches, that is, the side branches exhibited no variation with respect to ablation after 200 pulses. The laser field exhibited a similar shape. Therefore, laser-induced plasma was formed by the focused laser with the same field, thus ensuring that peak electron density approached an invariant point and did not change.

4. Conclusion and outlook

In conclusion, the evolution of laser-induced plasma through multipulse ablation in fused silica and the effect of a prepulse-induced crater on the subsequent laser field were studied using pump-probe technology. Filament splitting was observed in the early stage of plasma evolution (~300 fs) because the prepulse-induced crater reshaped the subsequent laser field with the competition between laser-divergent propagation caused by refraction and the self-focusing effect, which was validated by experiments and simulation results. The strongest laser focus was observed twice with the increasing pulse number during the process of subsequent propagation because of an optical path difference between the pulses from the center and edge areas of the crater. Divergent propagation of the laser generated a hole with branches. When the pulse number exceeded a particular value, which was 200 in the

Optics EXPRESS

experiments, the laser-induced electron density saturation was observed, which illustrated the hole branch structures were unchanged, thereby maintaining the same focused laser field. The experimental results reveal the formation mechanism of branches on the sides of the hole, which regulate laser–material interactions and improve the quality of processing during ultrafast multiple-pulse laser ablation.

Funding

National Key R&D Program of China (2017YFB1104300) and National Natural Science Foundation of China (11704028).

References

1. W. J. Yang, P. G. Kazansky, and Y. P. Svirko, "Non-reciprocal ultrafast laser writing," Nat. Photonics **2**(2), 99–104 (2008).
2. J. D. Steinmeyer, C. L. Gilleland, C. Pardo-Martin, M. Angel, C. B. Rohde, M. A. Scott, and M. F. Yanik, "Construction of a femtosecond laser microsurgery system," Nat. Protoc. **5**(3), 395–407 (2010).
3. A. Plech, V. Kotaidis, M. Lorenc, and J. Boneberg, "Femtosecond laser near-field ablation from gold nanoparticles," Nat. Phys. **2**(1), 44–47 (2006).
4. S. X. Wang, H. H. Yu, and H. J. Zhang, "Band-gap modulation of two-dimensional saturable absorbers for solid-state lasers," Photon. Res. **3**(2), A10–A20 (2015).
5. S. H. Chung and E. Mazur, "Surgical applications of femtosecond lasers," J. Biophotonics **2**(10), 557–572 (2009).
6. J. Serbin, T. Bauer, C. Fallnich, A. Kasenbacher, and W. H. Arnold, "Femtosecond lasers as novel tool in dental surgery," Appl. Surf. Sci. **197**, 197–198 (2002).
7. M. Malinauskas, A. Žukauskas, S. Hasegawa, Y. Hayasaki, V. Mizeikis, R. Buividas, and S. Juodkazis, "Ultrafast laser processing of materials: from science to industry," Light Sci. Appl. **5**(8), e16133 (2016).
8. F. Potemkin, E. Mareev, Y. Bezsudnova, V. Platonenko, B. Bravy, and V. Gordienko, "Controlled energy deposition and void-like modification inside transparent solids by two-color tightly focused femtosecond laser pulses," Appl. Phys. Lett. **110**(16), 163903 (2017).
9. G. D. Tsibidis, C. Fotakis, and E. Stratakis, "From ripples to spikes: a hydrodynamical mechanism to interpret femtosecond laser-induced self-assembled structure," Phys. Rev. B Condens. Matter Mater. Phys. **92**(4), 041405 (2015).
10. S. Linic, U. Aslam, C. Boerigter, and M. Morabito, "Photochemical transformations on plasmonic metal nanoparticles," Nat. Mater. **14**(6), 567–576 (2015).
11. C. Liao, K. Fan, R. L. Xu, H. C. Zhang, C. G. Lu, Y. P. Cui, and J. Y. Zhang, "Laser-annealing-made amplified spontaneous emission of 'giant' CdSe/CdS core/shell nanocrystals transferred from bulk-like shell to quantum-confined core," Photon. Res. **3**(5), 200–205 (2015).
12. C. Kerse, H. Kalaycıoğlu, P. Elahi, B. Çetin, D. K. Kesim, Ö. Akçaalan, S. Yavaş, M. D. Aşık, B. Öktem, H. Hoogland, R. Holzwarth, and F. Ö. Ilday, "Ablation-cooled material removal with ultrafast bursts of pulses," Nature **537**(7618), 84–88 (2016).
13. A. Vogel, J. Noack, G. Hüttman, and G. Paltauf, "Mechanisms of femtosecond laser nanosurgery of cells and tissues," Appl. Phys. B **81**(8), 1015–1047 (2005).
14. L. Wang, Q. D. Chen, X. W. Cao, R. Buividas, X. Wang, S. Juodkazis, and H. B. Sun, "Plasmonic nano-printing: large-area nanoscale energy deposition for efficient surface texturing," Light Sci. Appl. **6**(12), e17112 (2017).
15. J. R. Vázquez de Aldana, C. Méndez, and L. Roso, "Saturation of ablation channels micro-machined in fused silica with many femtosecond laser pulses," Opt. Express **14**(3), 1329–1338 (2006).
16. F. Bauer, A. Michalowski, T. Kiedrowski, and S. Nolte, "Heat accumulation in ultra-short pulsed scanning laser ablation of metals," Opt. Express **23**(2), 1035–1043 (2015).
17. Q. S. Wang, L. Jiang, J. Y. Sun, C. J. Pan, W. N. Han, G. Y. Wang, H. Zhang, C. P. Grigoropoulos, and Y. F. Lu, "Enhancing the expansion of a plasma shockwave by crater-induced laser refocusing in femtosecond laser ablation of fused silica," Photon. Res. **5**(5), 488–493 (2017).
18. Q. S. Wang, L. Jiang, J. Y. Sun, C. J. Pan, W. N. Han, G. Y. Wang, F. F. Wang, K. H. Zhang, M. Li, and Y. F. Lu, "Structure-mediated excitation of air plasma and silicon plasma expansion in femtosecond laser pulses ablation," Research **2018**, 1 (2018).
19. K. Sokolowski-Tinten and D. von der Linde, "Generation of dense electron-hole plasmas in silicon," Phys. Rev. B Condens. Matter Mater. Phys. **61**(4), 2643–2650 (2000).
20. L. Jiang, A. D. Wang, B. Li, T. H. Cui, and Y. F. Lu, "Electrons dynamics control by shaping femtosecond laser pulses in micro/nanofabrication: modeling, method, measurement and application," Light Sci. Appl. **7**(2), 17134 (2018).
21. M. Sun, U. Eppelt, S. Russ, C. Hartmann, C. Siebert, J. Zhu, and W. Schulz, "Numerical analysis of laser ablation and damage in glass with multiple picosecond laser pulses," Opt. Express **21**(7), 7858–7867 (2013).

Optics EXPRESS

22. Y. Ito, R. Shinomoto, K. Nagato, A. Otsu, K. Tatsukoshi, Y. Fukasawa, T. Kizaki, N. Sugita, and M. Mitsuishi, "Mechanisms of damage formation in glass in the process of femtosecond laser drilling," Appl. Phys., A Mater. Sci. Process. **124**(2), 181 (2018).
23. C. J. Pan, L. Jiang, Q. S. Wang, J. Y. Sun, G. Y. Wang, and Y. F. Lu, "Temporal-spatial measurement of electron relaxation time in femtosecond laser induced plasma using two-color pump-probe imaging technique," Appl. Phys. Lett. **112**(19), 191101 (2018).
24. Q. Sun, H. Jiang, Y. Liu, Z. Wu, H. Yang, and Q. Gong, "Measurement of the collision time of dense electronic plasma induced by a femtosecond laser in fused silica," Opt. Lett. **30**(3), 320–322 (2005).
25. A. Couairon and A. Mysyrowicz, "Femtosecond filamentation in transparent media," Phys. Rep. **441**(2–4), 47–189 (2007).
26. O. Kosareva, J.-F. Daigle, N. Panov, T. Wang, S. Hosseini, S. Yuan, G. Roy, V. Makarov, and S. Leang Chin, "Arrest of self-focusing collapse in femtosecond air filaments: higher order Kerr or plasma defocusing?" Opt. Lett. **36**(7), 1035–1037 (2011).
27. X. Mao, S. S. Mao, and R. E. Russo, "Imaging femtosecond laser-induced electronic excitation in glass," Appl. Phys. Lett. **82**(5), 697–699 (2003).
28. C. J. Pan, L. Jiang, J. Y. Sun, Q. S. Wang, F. F. Wang, and Y. F. Lu, "The temporal-spatial evolution of electron dynamics induced by femtosecond double pulses," Jpn. J. Appl. Phys. **58**(3), 030901 (2019).
29. L. Sudrie, A. Couairon, M. Franco, B. Lamouroux, B. Prade, S. Tzortzakis, and A. Mysyrowicz, "Femtosecond laser-induced damage and filamentary propagation in fused silica," Phys. Rev. Lett. **89**(18), 186601 (2002).